

Intra-molecular charge ordering in the multi-molecular-orbital system (TTM-TTP) I_3

Marie-Laure Bonnet and Vincent Robert*

Université de Lyon, Laboratoire de Chimie, Ecole Normale Supérieure de Lyon, CNRS, 46 allée d'Italie, F-69364 Lyon, France

Masahisa Tsuchiizu*, Yukiko Omori, and Yoshikazu Suzumura

Department of Physics, Nagoya University, Nagoya 464-8602, Japan

(Dated: September 11, 2009)

Starting from the structure of the (TTM-TTP) I_3 molecular-based material, we examine the characteristics of frontier molecular orbitals using *ab initio* (CASSCF/CASPT2) configurations interaction calculations. It is shown that the singly-occupied and second-highest-occupied molecular orbitals are close to each other, *i.e.*, this compound should be regarded as a two-orbital system. By dividing virtually the [TTM-TTP] molecule into three fragments, an effective model is constructed to rationalize the origin of this picture. In order to investigate the low-temperature symmetry breaking experimentally observed in the crystal, the electronic distribution in a pair of [TTM-TTP] molecules is analyzed from CASPT2 calculations. Our inspection supports and explains the speculated *intra-molecular* charge ordering which is likely to give rise to low-energy magnetic properties.

I. INTRODUCTION

The preparation and characterization of molecule-based electronic conductors is one of the central issue in the research of molecular crystal systems. Typical materials are TTF-TCNQ and (TMTSF) $_2$ PF $_6$, where, in the latter, the first superconductivity behavior in molecular solids has been reported.¹ Recent hot topics in the research of molecular crystals is the realization of charge-ordering phenomena.² Since the pioneer work of Su *et al.* in polyacetylene,³ the charge trapping phenomenon has been much studied in Peierls transition issues.⁴ In that sense, quasi-one-dimensional chains have received much attention from experimental and theoretical points of view.^{5,6,7,8} Theoretical approaches which focus on a single highest-occupied-molecular orbital (HOMO) or lowest-unoccupied-molecular orbital (LUMO) have been successful in describing fascinating electronic ordered phase. Such a treatment can be justified since, in these conventional systems, the HOMO or LUMO levels are well-separated from the rest of the MOs spectrum.² Nevertheless, new types of molecular solids have been recently synthesized, for instance aiming at the metalization of the single-component molecular solids family $M(\text{tmdt})_2$ ($M = \text{Ni}, \text{Au}$).⁹ The molecular extension of the tmdt system is so large that a description based upon a single MO is questionable. As a matter of fact, *ab initio* calculations have been performed^{10,11,12} and an effective three-band Hubbard model has been proposed and succeeded in describing electronic structures.¹³ In this respect, the quasi one-dimensional molecular compound (TTM-TTP) I_3 ,^{14,15,16} where TTM-TTP=2,5-bis(4,5-bis(methylthio)-1,3-dithiol-2-ylidene)-1,3,4,6-tetrathiapentalene looks like a promising candidate to investigate the theory limitation of a single-MO approximation. The presence of an I_3^- counteranion is suggestive of formally organic [TTM-TTP] $^+$ cations in the crystal structure, *i.e.*, unpaired electrons localized within the organic moieties. The magnetic susceptibility^{17,18} and NMR measurements^{19,20} revealed phase transitions at finite temperature. Insulating and non-magnetic behaviors have been confirmed at low-temperature. Furthermore, based on Raman-scattering^{21,22,23} and X-ray measurements,²⁴ it has

been suggested that an asymmetric deformation of the [TTM-TTP] molecule occurs and charge disproportionation within the molecule is possible below a transition temperature. This novel charge-ordered (CO) state is different from the conventional CO state² and is called *intra-molecular* CO state.²³ This non-trivial phenomena observed in this particular compound may not be described using on a single-band description, *i.e.*, the present molecular assembly could give rise to a phenomenon beyond a concept expected from a knowledge of a single molecule although the trigger may be hidden in the properties of multi-molecular orbitals. Thus, there is a crucial need for theoretical description to rationalize the origin of such state. The purposes of our study is (i) to show that the energy of singly-occupied-molecular orbital (SOMO) and that of second-highest-occupied molecular orbital (HOMO-1) are quasi-degenerate, (ii) to clarify the origin of this quasi-degeneracy using an effective three-fragment model for the [TTM-TTP] molecule, and (iii) to show explicitly that the *intra-molecular* charge ordering actually occurs in the neighboring two-molecular system. With this goal in mind, multi-reference wavefunction-based *ab initio* calculations are performed to rationalize the electronic distribution in the (TTM-TTP) I_3 material.

II. MOLECULAR-ORBITALS OF THE [TTM-TTP] $^+$ ION

The [TTM-TTP] organic molecule $C_{14}S_{12}H_{12}$ is shown in Fig. 1. The atomic coordinates are read from the (TTM-TTP) I_3 298 K crystal structure without performing any geometry optimization.¹⁵ Based on this structure, we performed explicitly correlated *ab initio* calculations. This type of approach is very insightful since important information is accessible through a reading of the wavefunction. In particular, complete active space self-consistent field (CASSCF) calculations have turned out to be very efficient to unravel intriguing electronic distribution in organic radical-based materials.^{25,26,27} On top of the CASSCF wavefunctions, second-order perturbation theory calculations (CASPT2) were performed using an imaginary shift = 0.3 a.u. and an IPEA shift = 0.0 a.u. This procedure allows one to incorporate the important dy-

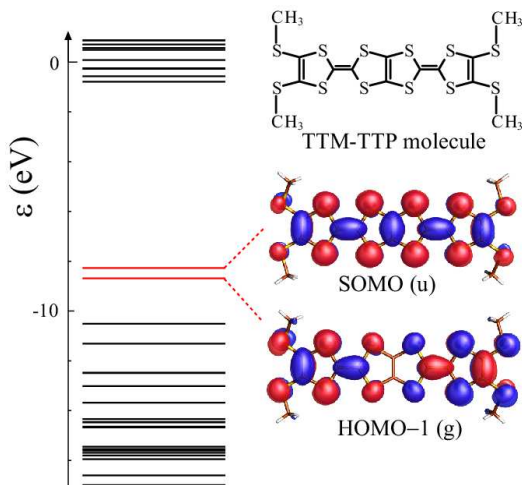


FIG. 1: (color) [TTM-TTP] molecule (right-top) and energy levels of the isolated [TTM-TTP]⁺ ion from ROHF *ab initio* SCF calculations. The SOMO (u) and HOMO-1 (g) are drawn where the red and blue colors denote the sign of wavefunction.

namical correlation effects to reach spectroscopic accuracy. All our *ab initio* calculations were performed using the MOL-CAS package²⁸ with all electron basis sets contractions for the elements S(7s6p1d)/[4s3p1d], C(5s5p1d)/[3s2p1d] and H(3s)/[1s]. We checked the validity of these particular contractions by including diffuse and polarization functions which did not lead to any quantitative changes.

At room-temperature, the [TTM-TTP] molecule exhibits an inversion center. Thus, the molecular orbitals (MOs) can be classified as gerade (g) or ungerade (u) according to the symmetry point group. As mentioned before, the (TTM-TTP)I₃ material is a charge-transfer salt, consisting of [TTM-TTP]⁺ and I₃⁻ species. In a simple picture, the HOMO of the [TTM-TTP]⁺ ion is half-filled, i.e., SOMO. It has been usually recognized that one may concentrate on this SOMO, ignoring the rest of the spectrum on the assumption that its energy is well-isolated from those of the other orbitals as compared to the band width.¹⁶ This is one particular issue we wanted to examine. Thus, semi-empirical extended Hückel calculations were first performed.^{29,30} In the following, the SOMO and HOMO-1 will be referred to as the u and g orbitals, respectively (see Fig. 1). The energy separation between the g and u valence MOs (see Fig. 1) is ≈ 0.2 eV, while the bandwidth of the HOMO is ≈ 1 eV.¹⁶ Thus, the effect of the g orbital might not be negligible since it is likely to participate in the intramolecular CO phenomenon expected in the (TTM-TTP)I₃ system. In order to clarify the charge distribution, CASSCF calculations were then carried out allowing the occupation of 2 MOs by 3 electrons, i.e., CAS[3,2]. This method is known to provide very satisfactory charge distribution as soon as the active space is flexible enough. The g and u MOs are then treated on the same footing and both symmetries states can be examined along these calculations. The CASSCF energy difference between the g and u doublets is ≈ 0.5 eV, confirming the relative proximity of the frontier orbitals. However, their energies are not directly accessible through CASSCF calcula-

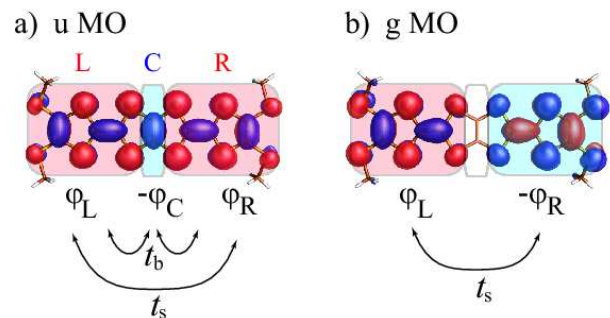


FIG. 2: (color) Effective three-fragment model for the u MO (a) and the g MO (b). The three fragments are named as L, R, and C, representing the left, right, and center fragments, and their wavefunctions are φ_L , φ_R , and φ_C , respectively. The u MO is given by the superposition of φ_L , $-\varphi_C$, and φ_R , while the g MO is made of φ_L and $-\varphi_R$. The mutual interaction between the respective fragments are t_b and t_s , representing the through-bond and through-space interactions, respectively.

tions. Thus, the energy spectrum was finally calculated using a restricted open-shell SCF procedure (ROHF). Along these ROHF calculations, three electrons are likely to occupy the frontier MOs u and g. The occupation numbers were set to 1.5 in order to get an estimate of the energies of the expected levels. The calculated energy levels in the vicinity of the SOMO are shown in Fig. 1. From this inspection, the SOMO has ungerade character, whereas the HOMO-1 is gerade type in agreement with our extended Hückel calculations. The respective ROHF energies $\varepsilon_u = -8.27$ eV and $\varepsilon_g = -8.69$ eV, while the energy difference between the u and g MOs is ≈ 0.4 eV, a value which is consistent with our extended Hückel estimation. This combined semi-empirical and *ab initio* information upon the constitutive unit [TTM-TTP]⁺ raises the relevance of a 1-band approach to examine the electronic properties of (TTM-TTP)I₃ crystal.

III. EFFECTIVE THREE-FRAGMENT MODEL

In this section, we analyze the chemical origin of the close-in-energy character of the g and u MOs. Let us split the [TTM-TTP] molecule into 3 fragments L, R, and C, as shown in Fig. 2. The L and R parts represent the left and right parts of the [TTM-TTP] molecule, whereas C corresponds to the ethylene-type bridging moiety. Based on this fragments picture, the u MO displays “bonding” character while the g MO “anti-bonding”. Therefore, one may wonder why the bonding MO lies higher in energy than the anti-bonding one. Part of the answer can be found in the C group orbital u which is likely to mix in the L-R “bonding” orbital (see Fig. 2). As for the interaction between these fragments, we here consider two types of hopping integrals, namely t_b and t_s . The former accounts for the through-bond interaction, while the latter represents the through-space interaction. The energy levels of the isolated L and R fragments are identical, and set to ε_0 . On the other hand, the energy level of the isolated C fragment is

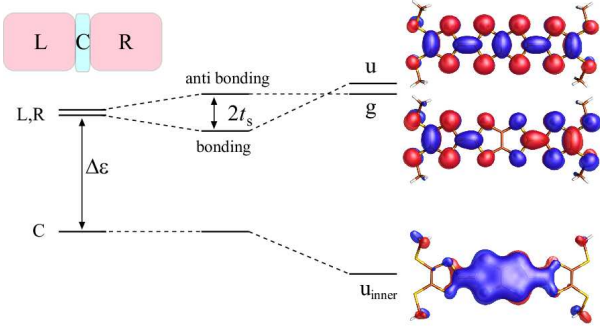


FIG. 3: (color) MOs diagram for the effective three-fragment model of the [TTM-TTP] molecule. As the through-space interaction t_s is turned on, the L and R local orbitals mix in and result in bonding and anti-bonding MOs (center). Then, the through-bond interaction t_b pushes the bonding MOs higher in energy (right). The identified MOs, u, g, and, u_{inner} , which are obtained from the SCF calculations, are also shown. The respective eigen-energies are given by $\varepsilon_u = -8.27$ eV, $\varepsilon_g = -8.69$ eV, and $\varepsilon_{u_{\text{inner}}} = -19.59$ eV.

much lower than the L and R fragments, and we parametrize the energy difference as $\Delta\varepsilon$ (> 0). Using the local orbitals φ_L , φ_R , and φ_C shown in Fig. 2, the effective Hamiltonian for the 3-fragment model reads

$$\begin{pmatrix} \varepsilon_0 & -t_s & -t_b \\ -t_s & \varepsilon_0 & -t_b \\ -t_b & -t_b & \varepsilon_0 - \Delta\varepsilon \end{pmatrix} \begin{matrix} L \\ R \\ C \end{matrix} \quad (1)$$

First, let us neglect the through-bond t_b interaction. The through-space interaction between the L and R parts results in bonding and anti-bonding MOs whose energy difference is $2t_s$. This virtual situation is shown in the center of Fig. 3. As soon as the t_b interaction is turned on, the energy of the bonding MO is shifted higher, while the anti-bonding MO remain unchanged due to symmetry constraints. Assuming that $\Delta\varepsilon$ is much larger than $|t_b|$, the eigenvalues read

$$\varepsilon_u \approx \varepsilon_0 - t_s + \frac{2t_b^2}{\Delta\varepsilon}, \quad (2a)$$

$$\varepsilon_g = \varepsilon_0 + t_s, \quad (2b)$$

$$\varepsilon_{u'} \approx \varepsilon_0 - \Delta\varepsilon - \frac{2t_b^2}{\Delta\varepsilon}. \quad (2c)$$

The respective wavefunctions are given by

$$\varphi_u = \frac{1}{\sqrt{2+a^2}}[(\varphi_L + \varphi_R) - a\varphi_C], \quad (3a)$$

$$\varphi_g = \frac{1}{\sqrt{2}}(\varphi_L - \varphi_R), \quad (3b)$$

$$\varphi_{u'} = \frac{-1}{\sqrt{1+a^2/2}} \left[\varphi_C + \frac{a}{2}(\varphi_L + \varphi_R) \right], \quad (3c)$$

where the quantity a is given by $a \approx (2t_b/\Delta\varepsilon)$. In this picture, the L, R and C fragments wavefunctions are assumed to be orthogonal which is obviously not a limitation for the

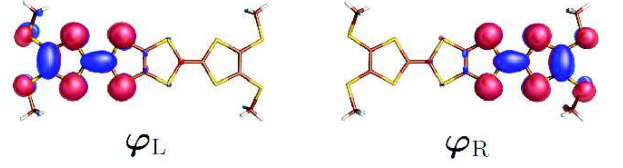


FIG. 4: (color) The L and R MOs obtained through a unitary transformation of Eq. (3) by taking $a = 0.25$.

description. By comparing Eq. (3) with the u and g MOs shown in Fig. 1, one can conclude distinctly that the wavefunctions φ_u and φ_g correspond to the u and g MOs, respectively. To scope out the $\varphi_{u'}$ MO which is given in Eq. (3c), we look into the set of ungerade MOs obtained from the SCF calculations. The in-phase combination u_{inner} of φ_L , φ_R , and φ_C wavefunctions is shown in Fig.3 and its energy is $\varepsilon_{u_{\text{inner}}} = -19.59$ eV. Since a typical value for $|t_b|$ is of the order of several eV, the latter energy separation fully justifies the approximate expressions given previously. Thus, we can assign the $\varphi_{u'}$ wavefunction to the u_{inner} MO identified in the SCF calculations.

The ratio $2t_b/\Delta\varepsilon$ ($\approx a$) was estimated from the charge distribution in the [TTM-TTP]⁺ ion, *i.e.*, so-called Mulliken charges. Based upon the CAS[3,2] wavefunctions, CASPT2 calculations were performed and the resulting Mulliken charges were estimated. Following the three-fragment model, we summed up the Mulliken charges within each fragment, *e.g.*, $\rho_L = \sum_{i \in L} \rho_i$ where i is the atom index. In the ground-state configuration where the u MO is singly occupied, the Mulliken charges on the respective fragments of the [TTM-TTP]⁺ ion were estimated as

$$\rho_L = \rho_R = +0.634, \quad \rho_C = -0.268. \quad (4)$$

The total charge is $\rho_L + \rho_R + \rho_C = +1$. In order to extract the contribution from the SOMO, we analyzed the charge difference between the cation [TTM-TTP]⁺ and the [TTM-TTP] molecule. The latter exhibits the following Mulliken charges on the respective fragments $\rho_L^0 = \rho_R^0 = +0.149$ and $\rho_C^0 = -0.297$. Thus, the charge differences $\Delta\rho_Z \equiv (\rho_Z - \rho_Z^0)$ ($Z = L, R, C$) were calculated as

$$\Delta\rho_L = \Delta\rho_R = 0.485, \quad \Delta\rho_C = 0.029. \quad (5)$$

This means that the hole is mainly localized on the L and R fragments, whereas the charge on the C fragment remains almost unchanged. By combining the information upon the SOMO [Eqs. (3a)] and the numerical data of the charge distribution [Eq. (5)], we can estimate the parameter $a \approx (2t_b/\Delta\varepsilon)$ by using the relations $1/(2+a^2) = \Delta\rho_L$ or $a^2/(2+a^2) = \Delta\rho_C$. Based on this analysis, we find $a \approx 0.25$ and finally the ratio $(t_b/\Delta\varepsilon)$ is ≈ 0.12 . Once the parameter a is determined, the fragment wavefunctions can be obtained explicitly through the inverse unitary transformation of Eq. (3). The resulting L and R MOs are shown in Fig. 4 and correspond to the φ_L and φ_R local MOs. Since $[(\varepsilon_u + \varepsilon_g)/2 - \varepsilon_{u_{\text{inner}}}] = \Delta\varepsilon[1 + 3(t_b/\Delta\varepsilon)^2]$ (see Eq. (2)), the ROHF eigenvalues $\varepsilon_u = -8.27$ eV, $\varepsilon_g = -8.69$ eV, and $\varepsilon_{u_{\text{inner}}} = -19.59$ eV

lead to the effective energy of the C fragment $\Delta\varepsilon \approx 10.6$ eV. Finally, the magnitudes of the through-bond/through-space interactions can be estimated, $t_b \approx 1.32$ eV and $t_s \approx -0.04$ eV. From our evaluation, t_s is almost negligible, and the bonding and antibonding MOs of Fig. 3 are almost degenerated. The through-space integral is much smaller than the through-bond one, $|t_b/t_s| \approx 28$. Since the energy difference between the u and g MOs is determined from Eq. (2)

$$\varepsilon_u - \varepsilon_g \approx -2t_s + \frac{2t_b^2}{\Delta\varepsilon}, \quad (6)$$

the origin of the quasi-degeneracy of the u and g MOs can be clarified in the light of the extracted parameters.

In conclusion, the u and g MOs ordering is completely determined by the relative energetics of this three-piece molecule. The through-space interaction t_s is almost negligible, while through-bond interaction t_b determines the energy spectrum.

IV. INTRA-MOLECULAR CHARGE ORDERING

In this section, the interactions between neighboring [TTM-TTP]⁺ cations have been investigated using a dimer extracted from the (TTM-TTP)₃ crystal. Since we were not only interested in charge distribution, CASPT2 calculations were also performed to specify the low-energy spectroscopy of the [TTM-TTP]₂²⁺ dimer.

A. “Molecular orbitals”

First, CASSCF calculations were carried out upon the [TTM-TTP]₂²⁺ dimer. These calculations were performed including 6 electrons in 4 MOs in the active space (CAS[6,4]) to account for the important static correlation effects. The interactions between the neighboring [TTM-TTP]⁺ ions labeled as **I** and **II** give rise to the effective “molecular orbitals” shown in Fig. 5. Importantly, the dimer exhibits an inversion center and the resulting MOs can be classified into *gerade* and *ungerade*. Nevertheless, the inversion center of each individual subunit is lost, which might lead to electron localization within the [TTM-TTP]⁺ building blocks. As expected, the CAS[6,4]SCF frontier orbitals (Fig. 5) consist in the in-phase and out-of-phase combinations of the $\varphi_{L,I}$, $\varphi_{R,I}$, $\varphi_{L,II}$, and $\varphi_{R,II}$ MOs. The $\varphi_{L,I}$ and $\varphi_{R,I}$ are the left (L) and right (R) localized MOs on the subunit **I** (see Fig. 4). A similar definition holds for the subunit **II**.

From the subsequent CASPT2 treatment, the ground state is a gerade singlet, and the active MOs exhibit occupation numbers 2.0, 2.0, 0.9, and 1.1, respectively. Importantly, the occupation numbers of the g_2 and u_2 MOs strongly deviate from 2 and 0, a feature of the open-shell nature of the ground state singlet. The symmetry breaking within each [TTM-TTP]⁺ ion induced by the presence of a second partner leads to a mixing of the orbitals depicted in Fig. 3. This particular mechanism is likely to result in the charge ordering we now wish to examine.

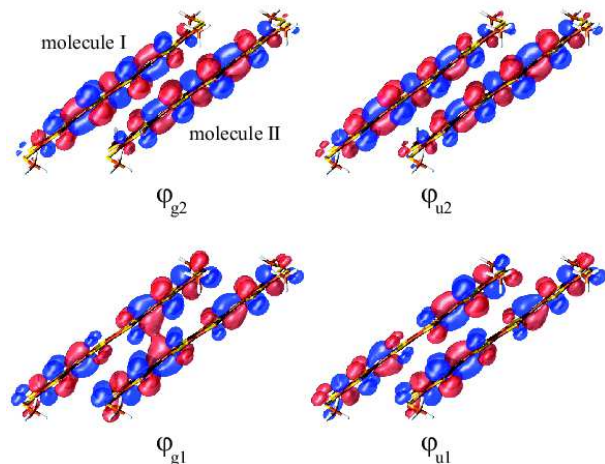


FIG. 5: (color) Valence MOs of the [TTM-TTP]₂²⁺ system obtained from CAS[6,4]SCF *ab initio* calculations upon the singlet state of g symmetry.

B. Mulliken charge

From the CASPT2 calculations performed upon the [TTM-TTP]₂²⁺ dimer, a similar Mulliken charge analysis was carried out to quantify the charge redistribution accompanying the dimer formation. The ground singlet state exhibits the following charge reorganization as compared to the isolated neutral [TTM-TTP] molecule

$$\Delta\rho_L = 0.272, \quad \Delta\rho_R = 0.697, \quad \Delta\rho_C = 0.030. \quad (7)$$

As a major conclusion, the charge on the left (right) fragment is strongly enhanced (reduced), which is a clear indication of the intra-molecular charge ordering. Again, the charge on the center fragment C is almost unchanged. The present evaluation based on the two-molecule dimer overestimates the charge difference between the L and R fragments as compared to its value in the crystal, and also the validity of Mulliken charges remains questionable since the fluctuation effects were not included. Nevertheless, this qualitative analysis supports the intra-molecular CO state.

C. Raman frequencies

In order to complement our previous charge analysis, Raman and IR calculations were performed using the Gaussian03 package³¹ on one and two-molecule systems using a BLYP functional and a triple zeta basis set. Our goal is to support the experimental conclusions which anticipated a symmetry breaking within the constitutive unit as the temperature is reduced. As a matter of fact, it has been observed upon cooling that the Raman 1486 cm⁻¹ band splits into two peaks centered at 1488 cm⁻¹ and 1498 cm⁻¹ (see Table I). This phenomenon was attributed to the differentiation between the C=C ylidene bonds, featuring a symmetry breaking.²¹ Thus, full geometry optimizations were carried out on both sys-

TABLE I: Calculated Raman vibrational frequencies for the one and two-molecule compounds. The former (latter) value is compared to the high-temperature (low-temperature) experimental data.^{22,23} All values are in cm^{-1} .

	calculated		experimental	
high-temperature	1535		1486	
low-temperature	1522	1534	1487	1500

tems. The information extracted from the one-molecule system should be compared with the high-temperature regime. In contrast, the two-molecule system is expected to give access to the low-temperature Raman spectrum characteristics.

Upon geometry optimization, the "left-right" symmetry of the constitutive TTM-TTP molecule in the 2-molecule system is lost. Then, despite a general blue-shift, the calculated Raman frequencies afford an interpretation of the temperature-induced phenomenon (see Table I). As a matter of fact, the low-temperature spectrum displays two peaks, in agreement with experimental data. Thus, this observation can be attributed to an intra-molecular CO phase accompanying the descent in symmetry within the TTM-TTP units. Our calculations confirm the propensity for such ordering which arises from inter-molecular interactions.

D. Low-energy spectroscopy

Our Mulliken charge analysis and Raman inspection are suggestive of an intra-molecular charge-ordering mechanism in the $(\text{TTM-TTP})\text{I}_3$ material. Thus, one may expect a charge localization on the left or right parts of the TTM-TTP building blocks. Such scenario is likely to give rise to magnetic interactions involving either the inner parts (*i.e.* $\varphi_{\text{R,I}}$ and $\varphi_{\text{L,II}}$ fragments MOs) or the outer parts (*i.e.* $\varphi_{\text{L,I}}$ and $\varphi_{\text{R,II}}$).

Thus, starting from the CAS[6,4]SCF calculations, the low-energy spectroscopy of the $[\text{TTM-TTP}]_2^{2+}$ species was inspected. The multi-reference CASSCF wavefunctions were expanded using a local orbitals basis set $\{\varphi_{\text{L,I}}, \varphi_{\text{R,I}}, \varphi_{\text{L,II}}, \varphi_{\text{R,II}}\}$ following the transformation

$$\varphi_{\text{g1}} \approx \frac{1}{2}(-\varphi_{\text{L,I}} + \varphi_{\text{R,I}} - \varphi_{\text{L,II}} + \varphi_{\text{R,II}}), \quad (8a)$$

$$\varphi_{\text{u1}} \approx \frac{1}{2}(+\varphi_{\text{L,I}} - \varphi_{\text{R,I}} - \varphi_{\text{L,II}} + \varphi_{\text{R,II}}), \quad (8b)$$

$$\varphi_{\text{g2}} \approx \frac{1}{2}(-\varphi_{\text{L,I}} - \varphi_{\text{R,I}} + \varphi_{\text{L,II}} + \varphi_{\text{R,II}}), \quad (8c)$$

$$\varphi_{\text{u2}} \approx \frac{1}{2}(+\varphi_{\text{L,I}} + \varphi_{\text{R,I}} + \varphi_{\text{L,II}} + \varphi_{\text{R,II}}). \quad (8d)$$

Since we are dealing with a 6-electron/4-MO system, we performed our analysis in the 2-hole/4-MO picture. Schematic representations of the different hole configurations for the singlet and triplet states based on these local orbitals are shown in Fig. 6. Such transformation affords a reading of the different wavefunctions and the extractions of the relevant information in a valence-bond type analysis. Since $|t_s|$ is relatively small, the left and right moieties within each unit do not significantly overlap. Thus, the previous transformation is almost unitary.

The lowest lying states of the $[\text{TTM-TTP}]_2^{2+}$ species are given in Table II. The ground state is singlet g and consistent with picture that minimizes the electrostatic energy between the two $[\text{TTM-TTP}]^+$ ions, each including 3 electrons. The comparison between the ground state singlet g and first triplet u is very instructive. In both cases, the wavefunction is dominated by electronic configurations (0.66 and 0.93 in Table II for the singlet and triplet states, respectively) involving the inner parts (see Fig. 6). Therefore, the energy difference affords an evaluation of the intermolecular magnetic exchange interaction :

$$J \equiv E_1 - E_0 \approx 0.09 \text{ eV} \quad (9)$$

A positive value reflects an antiferromagnetic interaction, resulting from the intra-molecular charge ordering. Such a value suggests that the spin gap excitation energy should be ≈ 900 K. The first-excited singlet corresponds to the holes localization within one $[\text{TTM-TTP}]^+$ ion. This is a reflection of an *inter-molecular* charge ordering which lies much higher and might not be relevant to describe the low-energy properties of the $(\text{TTM-TTP})\text{I}_3$ material. The energy difference (0.35 eV) between this second excited state (singlet g) and the fourth one (triplet u) supports the strong antiferromagnetic interaction within each subunit. This is a mechanism that involves again inter-molecular electron transfer. Finally, the nature of the third excited state (triplet u) is rather puzzling. From the intra-molecular charge ordering, the $|\varphi_{\text{L,I}}\varphi_{\text{R,II}}\rangle$ configuration is unfavorable as a result of the electrostatic repulsions. The low-energy spectroscopy in the $(\text{TTM-TTP})\text{I}_3$ material should be mostly governed by the through-space inter-dimer magnetic interaction J , which results from the intra-molecular charge ordering.

V. SUMMARY

In the present paper, we examined the low-energy properties of the $(\text{TTM-TTP})\text{I}_3$ material. Complementary semi-empirical and wavefunction-based *ab initio* calculations were

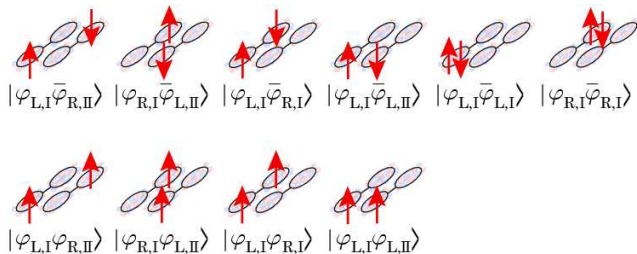


FIG. 6: (color) Schematic view of the different configurations using a hole picture for the singlet (top) and triplet (bottom), respectively. The subscripts I and II stand for the molecules I and II as depicted in Fig. 5.

TABLE II: Wavefunctions decompositions (weights) of the $[\text{TMM-TTP}]_2^{2+}$ low-energy states. The wavefunctions are expressed in terms of the 2-hole determinants. CAS[6,4]PT2 energies with respect to the ground state singlet g are given in eV.

	$ \varphi_{L,I} \bar{\varphi}_{R,II}\rangle$	$ \varphi_{R,I} \bar{\varphi}_{L,II}\rangle$	$ \varphi_{L,I} \bar{\varphi}_{R,I}\rangle$	$ \varphi_{L,I} \bar{\varphi}_{L,II}\rangle$	$ \varphi_{L,I} \bar{\varphi}_{L,I}\rangle$	$ \varphi_{R,I} \bar{\varphi}_{R,I}\rangle$	energy (eV)
singlet, gerade	0.03	0.66	0.04	0.06	0.06	0.14	$E_0 = 0.00$
	0.01	0.01	0.91	0.03	0.00	0.04	$E_2 = 0.27$

	$ \varphi_{L,I} \varphi_{R,II}\rangle$	$ \varphi_{R,I} \varphi_{L,II}\rangle$	$ \varphi_{L,I} \varphi_{R,I}\rangle$	$ \varphi_{L,I} \varphi_{L,II}\rangle$	energy (eV)
triplet, ungerade	0.03	0.93	0.00	0.04	$E_1 = 0.09$
	0.61	0.00	0.07	0.31	$E_3 = 0.47$
	0.05	0.00	0.93	0.03	$E_4 = 0.62$

performed upon the elementary unit and a dimer to investigate the underlying electronic distribution. We showed that the SOMO and HOMO-1 are close in energy and that a one-band picture should be ruled out. A chemical understanding arises from the inspection of the building block and effective parameters extracted from a three-fragment model allowed us to rationalize the quasi-degeneracy of the [TMM-TTP] frontier MOs. From the calculation of a system consisting of two neighboring molecules, the inversion symmetry within each molecule is lost. This result is in agreement with experimental data. Indeed, the intra-molecular charge ordering which has been experimentally suggested actually occurs in the 2-molecule cluster system. The mixing of the SOMO and HOMO-1 results in an electron trapping which results in a 0.697 / 0.272 on the L / R moieties of the $[\text{TMM-TTP}]^+$ ion. To complement the anticipated scenario, Raman frequencies have been calculated and agree on a charge disproportionation within each $[\text{TMM-TTP}]^+$ unit. Finally, our *ab initio* calculations suggest that the low-energy of the $(\text{TMM-TTP})\text{I}_3$ ma-

terial is controlled by a single exchange interaction 0.09 eV, resulting from the charge ordering.

Acknowledgments

MT thanks T. Kawamoto, T. Mori, H. Kobayashi, for the fruitful discussions on the $(\text{TMM-TTP})\text{I}_3$ compounds. MLB, MT, YO, YS thank S. Ishibashi and H. Seo for the discussions on the theoretical aspects. MT thanks S. Yasuzuka for the enlightening discussions in the early stage of the present work. MLB was supported by the JSPS postdoctoral fellowship for Foreign Researchers. This research was partially supported by Nagoya University Science Foundation and Grant-in-Aid for Scientific Research on Innovative Areas (20110002) from the Ministry of Education, Culture, Sports, Science and Technology, Japan.

-
- ¹ D. Jerome and H.J. Schulz, *Adv. Phys.* **31**, 299 (1982).
² H. Seo, C. Hotta, and H. Fukuyama, *Chem. Rev.* **104**, 5005 (2004).
³ W.P. Su, J.R. Shrieffer, and A.J. Heeger, *Phys. Rev. Lett.* **42**, 1698 (1979).
⁴ R. Peierls, in *Quantum Theory of Solids* (Clarendon: Oxford, U.K. 1955).
⁵ S.A. Borshch, K. Prassides, V. Robert, and A.O. Solonenko, *J. Chem. Phys.* **109**, 4562 (1998).
⁶ V. Robert, S. Petit, S.A. Borshch, *Inorg. Chem.* **38**, 1573 (1999).
⁷ V. Robert, *J. Chem. Phys.* **121**, 4297 (2004).
⁸ J.-P. Malrieu, V. Robert, *J. Chem. Phys.* **120**, 7374 (2004).
⁹ H. Tanaka, Y. Okano, H. Kobayashi, W. Suzuki, and A. Kobayashi, *Science* **291** (2001) 285.
¹⁰ C. Rovira, J.J. Novoa, J.-L. Mozos, P. Ordejón, and E. Canadell, *Phys. Rev. B* **65** (2002) 081104.
¹¹ S. Ishibashi, H. Tanaka, M. Kohyama, M. Tokumoto, A. Kobayashi, H. Kobayashi, and K. Terakura, *J. Phys. Soc. Jpn.* **74**, 843 (2005).
¹² S. Ishibashi, K. Terakura, and A. Kobayashi, *J. Phys. Soc. Jpn.* **77** (2008) 024702.
¹³ H. Seo, S. Ishibashi, Y. Okano, H. Kobayashi, A. Kobayashi, H. Fukuyama, and K. Terakura, *J. Phys. Soc. Jpn.* **77**, 023714 (2008).
¹⁴ For a review, T. Mori, *Chem. Rev.* **104**, 4947 (2004).
¹⁵ T. Mori, H. Inokuchi, Y. Misaki, T. Yamabe, H. Mori, and S. Tanaka, *Bull. Chem. Soc. Jpn.* **67**, 661 (1994).
¹⁶ T. Mori, T. Kawamoto, J. Yamaura, T. Enoki, Y. Misaki, T. Yamabe, H. Mori, and S. Tanaka, *Phys. Rev. Lett.* **79**, 1702 (1997).
¹⁷ M. Maesato, Y. Sasou, S. Kagoshima, T. Mori, T. Kawamoto, Y. Misaki, and T. Yamabe, *Synth. Met.* **103**, 2109 (1999).
¹⁸ N. Fujimura, A. Namba, T. Kambe, Y. Nogami, K. Oshima, T. Mori, T. Kawamoto, Y. Misaki, and T. Yamabe, *Synth. Met.* **103**, 2111 (1999).
¹⁹ M. Onuki, K. Hiraki, T. Takahashi, D. Jinno, T. Kawamoto, T. Mori, T. Takano, and Y. Misaki, *Synth. Met.* **120**, 921 (2001).
²⁰ M. Onuki, K. Hiraki, T. Takahashi, D. Jinno, T. Kawamoto, T. Mori, K. Tanaka, and Y. Misaki, *J. Phys. Chem. Solids* **62**, 405 (2001).
²¹ K. Yakushi, R. Świetlik, K. Yamamoto, T. Kawamoto, T. Mori, Y. Misaki, and K. Tanaka, *Synth. Met.* **135**, 583 (2003).
²² R. Świetlik, K. Yakushi, K. Yamamoto, T. Kawamoto, and T. Mori, *J. Phys. IV France* **114**, 87 (2004).

- ²³ R. Świetlik, K. Yakushi, K. Yamamoto, T. Kawamoto, T. Mori, *Synth. Met.* **150**, 83 (2005).
- ²⁴ Y. Nogami, T. Kambe, N. Fujimura, K. Oshima, T. Mori, and T. Kawamoto, *Synth. Met.* **135-136**, 637 (2003).
- ²⁵ J.-B. Rota, L. Norel, C. Train, N. Ben Amor, D. Maynau, and V. Robert, *J. Am. Chem. Soc.* **130**, 10380 (2008).
- ²⁶ S. Messaoudi, V. Robert, N. Guihery, and D. Maynau, *Inorg. Chem.* **45**, 3212 (2006).
- ²⁷ M. Kepenekian, B. Le Guennic, K. Awaga, and V. Robert, *Phys. Chem. Chem. Phys.* in press DOI is available now (2009).
- ²⁸ G. Karlström *et al.*, *Comp. Mater. Sci.* **28** (2003) 222.
- ²⁹ T. Mori, A. Kobayashi, Y. Sasaki, H. Kobayashi, G. Saito, and H. Inokuchi, *Bull. Chem. Soc. Jpn.* **57**, 627 (1984).
- ³⁰ T. Mori, Doctor Thesis, Univ. Tokyo (1985), Chap. 4.
- ³¹ M.J. Frisch *et al.*, *Gaussian 03* (Gaussian, Inc., Pittsburgh PA, 2003).